Turbulent transport in premixed flames

By C. J. Rutland[1] AND R. S. Cant[2]

Simulations of planar, premixed turbulent flames with heat release were used to study turbulent transport. Reynolds stress and Reynolds flux budgets were obtained and used to guide the investigation of important physical effects. Essentially all pressure terms in the transport equations were found to be significant. In the Reynolds flux equations, these terms are the major source of counter-gradient transport. Viscous and molecular terms were also found to be significant, with both dilatational and solenoidal terms contributing to the Reynolds stress dissipation. The BML theory of premixed turbulent combustion was critically examined in detail. The BML bimodal pdf was found to agree well with the DNS data. All BML decompositions, through the third moments, show very good agreement with the DNS results. Several BML models for conditional terms were checked using the DNS data and were found to require more extensive development.

1. Introduction

The use of DNS to study turbulent premixed flames has proved to be very successful. Most of the previous work in this area has focused on turbulence effects on the flame structure and statistics. This has provided invaluable information and insight for formulating turbulent combustion models for the mean reaction rate (Bray & Cant, 1991, Trouvé & Poinsot, 1993).

As combustion models have advanced it is apparent that turbulence models require more attention. Most modern turbulent combustion models rely heavily on mixing and time-scale (strain rate) information from the turbulence models. Thus, it is critical to understand how turbulent transport is affected by premixed combustion.

A model formalism developed by Bray, Moss, and Libby (1985) provides a highly developed theoretical basis for turbulent premixed flames. It is based on a presumed, bi-modal pdf of the reaction progress variable that is readily obtained using DNS simulations. The BML theory has proved successful in predicting several properties of premixed flames including counter-gradient transport (Libby & Bray, 1981).

The purpose of the current work is to study the major physical effects of premixed flames on turbulent transport in the context of the BML formalism. The BML theory results in decompositions of higher moments in terms of conditional lower moments. This approach simplifies closure and is examined in detail. A variety

1 Department of Mechanical Engineering,University of Wisconsin-Madison

2 Department of Mechanical Engineering, UMIST, Manchester M60 1QD, United Kingdom

of terms in the BML theory require modeling approximations and these were also investigated. To provide data for this study, a direct simulation was made of a planar, turbulent premixed flame with heat release.

1.1. Simulation method and parameters

The flow configuration represents a planar turbulent flame shown schematically in Fig. 1. Turbulent flow enters at the left, passes through the flame brush, and exits at the right. The spanwise boundaries (y, z) are periodic and the flow is considered to be homogeneous in these directions. This configuration simplifies analysis of the results because most of the statistical information varies only in the streamwise direction.
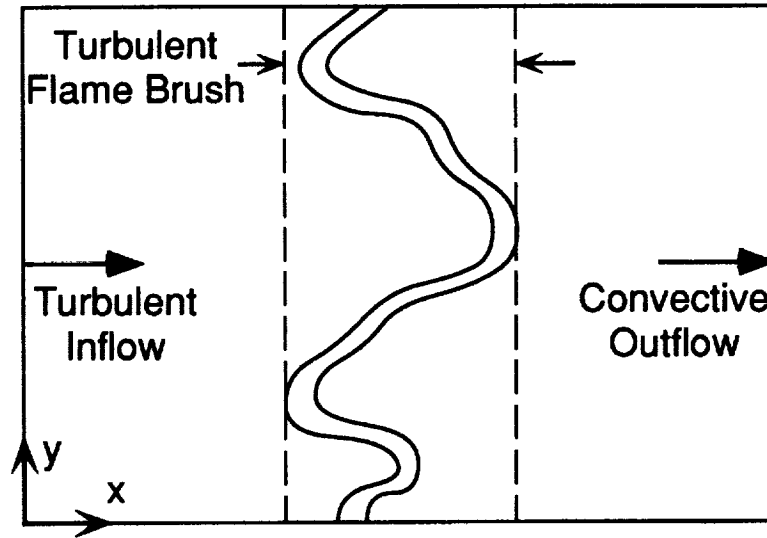
FIGURE 1. Schematic drawing of the computational domain and turbulent flame brush. The domain size is $5 \times 2\pi \times 2\pi$ and the grid size is 251 × 128 × 128.

The flame is considered to be premixed with a simple, single step, global reaction rate controlled by Arrhenius kinetics. Since the issues of interest concern only flame-turbulence interaction, acoustic energy is assumed to be unimportant and is removed from the equations using the low Mach number approximation (McMurtry et al., 1986). However, the reaction is exothermic and heat release effects are retained through density variations in both time and space. It is also assumed that the Lewis number is unity and that Soret and Dufour effects are negligible. This results in the following set of equations:

$$\frac{\partial \rho}{\partial t} + \frac{\partial \rho u_i}{\partial x_i} = 0 \tag{1}$$

$$\frac{\partial \rho u_i}{\partial t} + \frac{\partial \rho u_j u_i}{\partial x_j} = -\frac{\partial p}{\partial x_i} + \frac{\partial \tau_{ij}}{\partial x_j} \tag{2}$$

$$\frac{\partial \rho T}{\partial t} + \frac{\partial \rho u_j T}{\partial x_j} = \frac{1}{RePr}\frac{\partial^2 T}{\partial x_j \partial x_j} + \dot{\omega} \tag{3}$$

where

$$\tau_{ij} = \frac{1}{Re}\left[\left(\frac{\partial u_i}{\partial x_j} + \frac{\partial u_j}{\partial x_i}\right) - \frac{2}{3}\frac{\partial u_k}{\partial x_k}\delta_{ij}\right] \tag{4}$$

$$\rho\left[(\frac{\alpha}{1-\alpha})T + 1\right] = 1 \tag{5}$$

$$\dot{\omega} = B^*\rho(1 - T)\exp\left(\frac{-\beta(1 - T)}{1 - \alpha(1 - T)}\right) \tag{6}$$

The equations have been non-dimensionalized using the laminar flame speed, the domain size in the spanwise direction, the inlet density, and the inlet and adiabatic flame temperatures. The non-dimensional temperature varies between 0 and 1. Thus, for these unity Lewis number simulations, temperature is equivalent to the reaction progress variable, c.

The equations are solved using Fourier pseudo-spectral methods for the spanwise derivatives and a sixth order, compact finite difference scheme (Lele, 1990) for the streamwise derivatives. Heat release in the flame precludes the use of Fourier methods in the streamwise direction.

The low Mach number approximation results in an elliptic aspect to the problem that is satisfied using a Poisson equation derived from the pressure gradient and the continuity equation. The solution is obtained on a pressure grid that is staggered only in the streamwise direction to avoid difficulties with pressure boundary conditions. Time integration is carried out using a combination of explicit 3rd-order compact Runge-Kutta and implicit Crank-Nicolson methods. The viscous and diffusion terms are treated primarily with the implicit method, and the non-linear terms are integrated with the explicit method.

The turbulent inflow boundary is simulated by a pre-computed isotropic turbulent field. This turbulent field is generated using a specified energy spectrum, continuity, and random phases. The energy spectrum for the current work is given by (Schumann & Patterson, 1978):

$$E(k) = C_o \frac{k}{k_o^2}\exp\left(-\frac{k}{k_o}\right) \tag{7}$$

where $C_o = 3.0$ and $k_o = 5.0$. Using an approach developed by Lee *et al.* (1991), velocities are interpolated onto a plane moving through the isotropic field. This plane is used as the inflow boundary in the flame calculations. The outflow boundary uses a convection condition with corrections for global mass conservation (Rutland *et al.*, 1989). Additional information about the numerical methods can be found in Zhang (1994).

The problem parameters were chosen to satisfy several constraints. The primary consideration was to remain in the thin flame regime in which local, internal

flame structure is not significantly affected by the turbulence. From previous work (Rutland *et al.*, 1989), it was determined that the simulated flames are thin if the Karlovitz number, Ka, is approximately one or less, where:

$$Ka = \frac{\delta/S_L}{\lambda/u'} \tag{8}$$

Since at least 15 grid points are required to resolve the laminar flame structure, the thin flame requirement sets the basic grid spacing. In other words, grid resolution of the flame is more stringent than grid resolution of the turbulence. The flame was initiated as a laminar flame in a laminar flow field at the midpoint of the domain in the x-direction. At the start of the simulations, the turbulence at the inlet was rapidly, but smoothly, ramped-up to the inlet values reported in Table 1. As the calculation proceeded in time, the turbulence and flame interacted until a fairly stationary turbulent flame developed.

Table 1: Simulation and data set parameters

Problem parameters :

α, heat release parameter, Eq. (5)	$0.7; (\tau = 2.3)$
β, activation energy parameter, Eq. (6)	6.0
B^*, pre − exponential parameter, Eq. (6)	1225.9
Re, scaling Reynolds number, Eq. (3)	30
Pr, Prandtl number	0.7

Inlet turbulence parameters :

κ, kinetic energy	3.0
λ, Taylor microscale	0.18
L, integral length scale	1.35
Re_L, integral scale Reynolds number	56.7
Integral time scale	0.964

Data set information

time (non − dimensional)	4.57
time (turn over)	4.73
laminar flame thickness	0.173
turbulent flame speed	2.03
turbulent flame brush location	$x \approx 1.0 \ to \ 4.4$

2. Reynolds stress budget

In the one-dimensional turbulent flame configuration being studied, spanwise derivatives of mean quantities are zero. The primary Reynolds stress transport equation is for the $(i,j) = (1,1)$ term:

$$\frac{\partial \overline{\rho u_1'' u_1''}}{\partial t} + \frac{\partial \tilde{u} \overline{\rho u_1'' u_1''}}{\partial x_1} = -2\overline{\rho u_1'' u_1''}\frac{\partial \tilde{u}_1}{\partial x_1} - \frac{\partial \overline{\rho u_1'' u_1'' u_1''}}{\partial x_1} - 2\overline{u_1'' \frac{\partial \overline{p}}{\partial x_1}} + 2\overline{u_1'' \frac{\partial \tau_{1k}}{\partial x_k}} \tag{9}$$

In this basic form of the equation, the pressure and viscous terms have not been decomposed. Fig. 2 shows how the terms vary through the flame brush. We have adopted the convention that terms are plotted with their signs. Thus, terms from the right hand side of an equation are positive in the plots when the term is a source of the conserved quantity on the left hand side of the equation.
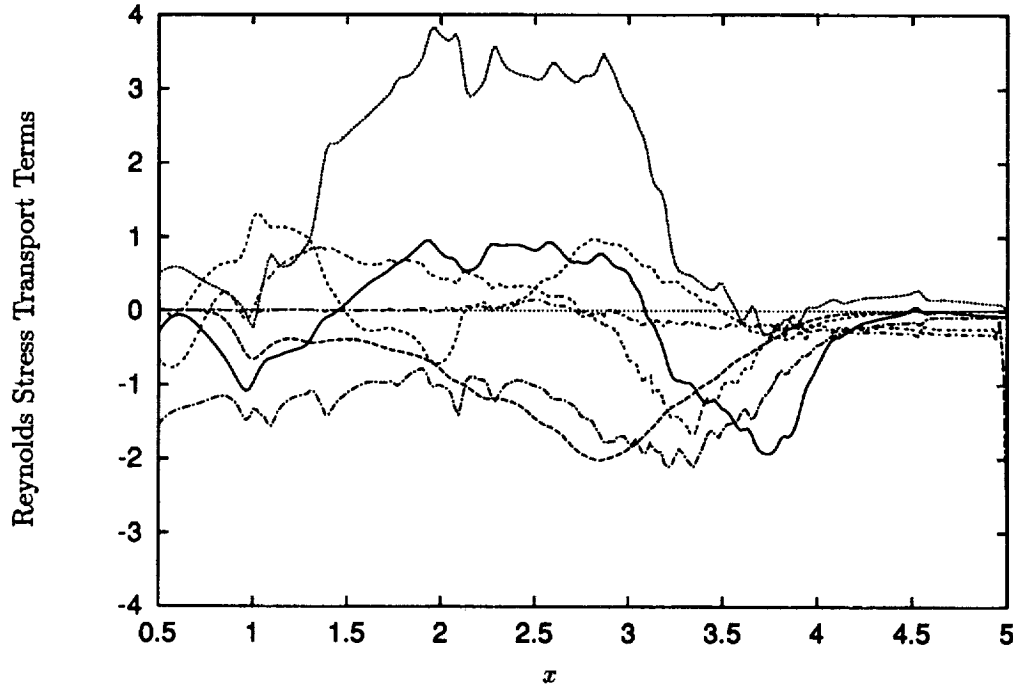

FIGURE 2. Reynolds stress budget, Eq. (9): convection term (———), production term (— — — —), triple correlation (- - - -), velocity-pressure gradient (········), viscous term (—·—·—), unsteady term (-- --- -), unclosed term (— - — - —).

The Reynolds stress budget in Fig. 2 includes the unsteady term and the 'unclosed' amount in the budget. The magnitude of the unclosed quantity is negligible except in the latter part of the flame brush. This comes from errors in estimating the unsteady term via a simple finite difference when density changes. The unsteady term is still significant, indicating that there is some growth in the flame brush as it moves towards higher turbulence levels. Despite the relatively large unsteady term, it is believed that the Reynolds stress budget accurately reflects the relative importance and magnitudes of the various terms.

Fig. 2 shows that the pressure term is the dominate source of turbulence. The major sinks are the dissipation and 'production' terms. Note that in this context the production term actually represents mean dilatation since there is no mean shear. In the following paragraphs, the pressure and viscous terms are decomposed following conventional procedures in second moment modeling (Jones, 1980). While there

is some indication that this approach could be revised for reacting flows (Strahle, 1983), we follow the convention of Bray *et al.* (1985).

The pressure terms are dominant sources of turbulence in the flame brush. Standard decomposition first separates the mean and fluctuating pressure. Then, the fluctuating term is rewritten as a transport term, a pressure-strain term, and a pressure dilatation term:

$$-\overline{2u_1''\frac{\partial p}{\partial x_1}} = -\overline{2u_1''}\frac{\partial \bar{p}}{\partial x_1} - 2\frac{\partial \overline{u_1''p'}}{\partial x_1} + \Phi_{11} + \frac{2}{3}\overline{p'\frac{\partial u_k''}{\partial x_k}} \tag{10}$$

where

$$\Phi_{ij} = \overline{p'\left(\frac{\partial u_i''}{\partial x_j} + \frac{\partial u_j''}{\partial x_i}\right)} - \frac{2}{3}\overline{p'\frac{\partial u_k''}{\partial x_k}}\delta_{ij} \tag{11}$$

Fig. 3 shows the variation of the pressure terms through the flame brush. The dominant terms appear to be the mean pressure term and the pressure transport term. The mean pressure gradient is always positive and increases turbulence. The pressure transport term changes sign from positive in the leading half of the flame brush to negative in the trailing half. The pressure dilatation is also an important source of turbulence throughout the flame brush. The pressure strain is fairly small and oscillates around zero through the flame.
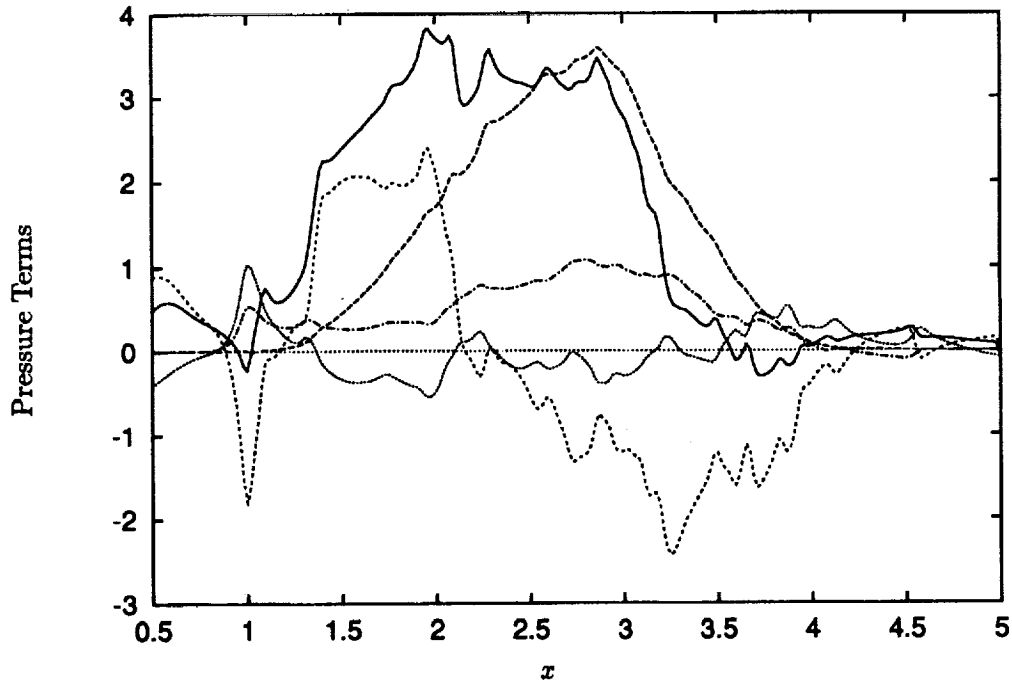

FIGURE 3. Pressure terms in the Reynolds stress budget, Eq. (10): total velocity-pressure gradient (————), mean pressure gradient (— — —), pressure transport (- - - - -), pressure strain (········), pressure dilatation (— — —).

In general, these results justify the standard decomposition for the pressure term. The mean pressure gradient is significant and can be obtained directly in second moment models. The pressure strain is small so that its modeling should be less critical in the flame zone. Pressure dilatation is important and new models have been suggested from other DNS results (Zhang & Rutland, 1994). The most troublesome term is the pressure transport term. It is unlikely that combining this term with other transport terms in a gradient diffusion model will be satisfactory in premixed flames.

The major sinks for turbulence are the mean dilatation and the viscous terms. Since the mean dilatation is readily obtained in second moment models, we will focus only on the viscous term. Conventional decomposition similar to that used for the pressure term leads to

$$
\overline{2u_1'' \frac{\partial \tau_{1k}}{\partial x_k}} = 2\frac{\partial \overline{u_1''\tau_{1k}}}{\partial x_k} - 2\overline{\tau_{1k}\frac{\partial \overline{u_1''}}{\partial x_k}} - \Pi_{11} - \frac{2}{3}\overline{\tau_{mk}' \frac{\partial u_m''}{\partial x_k}} \tag{12}
$$

where

$$
\Pi_{ij} = \overline{\tau_{ik}' \frac{\partial u_j''}{\partial x_k}} + \overline{\tau_{jk}' \frac{\partial u_i''}{\partial x_k}} - \frac{2}{3}\overline{\tau_{mk}' \frac{\partial u_m''}{\partial x_k}}\delta_{ij} \tag{13}
$$

This gives a turbulent transport term, a mean viscous term, a deviatoric term (Π_{ij}), and the dissipation function. Note that in the viscous stress, τ_{ij} is separated into a mean and fluctuating term using standard averaging instead of Favre averaging. This facilitates the separation of terms used in Eq. (12).

The variation of viscous terms through the flame brush are plotted in Fig. 4. This shows that the dissipation function dominates and the mean term is small, as expected. Interestingly, the transport term and the deviatoric term tend to have opposite signs and nearly balance each other in the leading half of the flame. It is unclear why this occurs. Recent work by Antonia *et al.* (1994) indicate that the anisotropy tensor for the dissipation function varies as the Reynolds stress anisotropy. This suggests that Π_{ij} might follow the Reynolds stress anisotropy. However, this was not found in the current reacting flow dataset since the Reynolds stress anisotropy increases through the flame brush while Π_{ij} decreases slightly.

Since the dissipation function dominates the viscous term, it is examined in more detail. This is facilitated by separating the term into solenoidal and dilatational terms as follows:

$$
\frac{2}{3}\overline{\tau_{ij}' \frac{\partial u_i''}{\partial x_j}} = \frac{2}{3Re}\left[2\overline{\hat{S}_{ij}'\hat{S}_{ij}'} + \frac{4}{3}\overline{\theta'\theta'}\right] \tag{14}
$$

where

$$
\hat{S}_{ij}' = \frac{1}{2}\left(\frac{\partial u_i'}{\partial x_j} + \frac{\partial u_j'}{\partial x_i}\right) - \frac{1}{3}\theta'\delta_{ij} \tag{15}
$$

$$
\theta' = \frac{\partial u_k'}{\partial x_k} \tag{16}
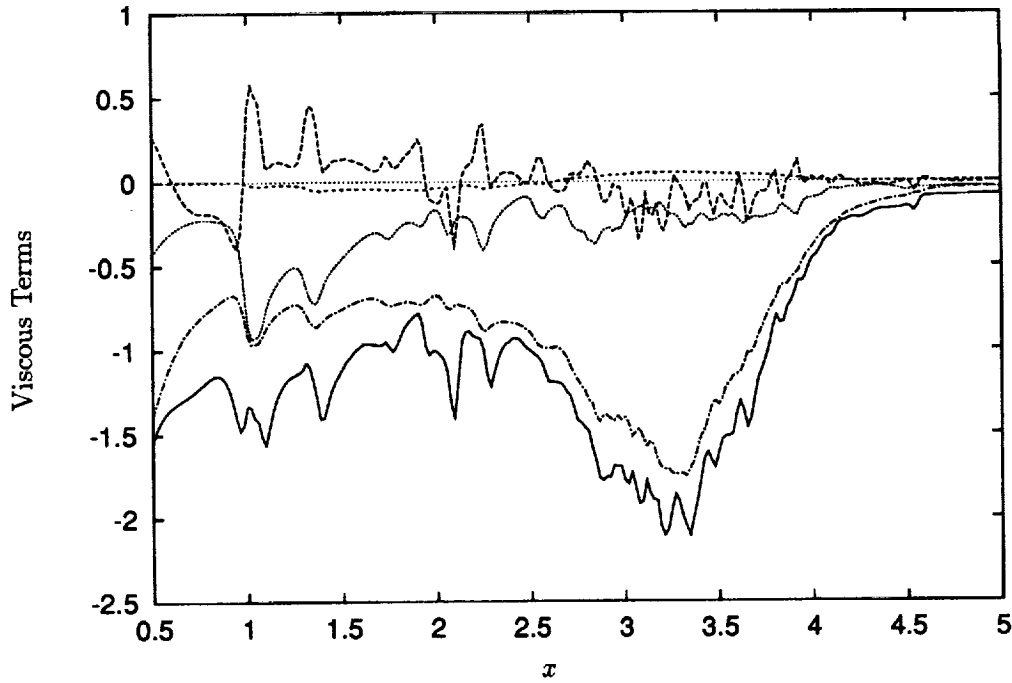$$

FIGURE 4.   Viscous terms in the Reynolds stress budget, Eq. (12): total viscous term (———), viscous stress transport (— — —), mean viscous stress gradient term (- - - - -), deviatoric term (·······), dissipation function (— ·· — ·· —).

This result uses the symmetry of τ_{ij}' and the relationship:

$$\overline{g'h''} = \overline{g'h'} \tag{17}$$

Note that the solenoidal term is not purely homogeneous. However, comparisons with the homogeneous dissipation calculated using enstrophy have shown the non-homogenous contributions to be small in the current data set. Thus, the main contribution to the solenoidal term is from vorticity.

Fig. 5 shows the variation of the dissipation terms through the flame brush. The dilatational dissipation is significant throughout and dominates in the leading half of the flame brush. The solenoidal dissipation becomes significant in the latter half of the flame brush. This was found to coincide with increasing vorticity generation by baroclinic torque.

Since the only dilatation in the flow occurs at the local flame sheet, the dilatational dissipation comes exclusively from this region. This was confirmed by evaluating the dilatational dissipation conditioned on the progress variable so that contributions from the reactants, flame zone, and products could be determined. This is important since the modeling of terms that are due to the local flame sheet can be fairly straightforward provided the mean reaction rate (or flame sheet density) is known.
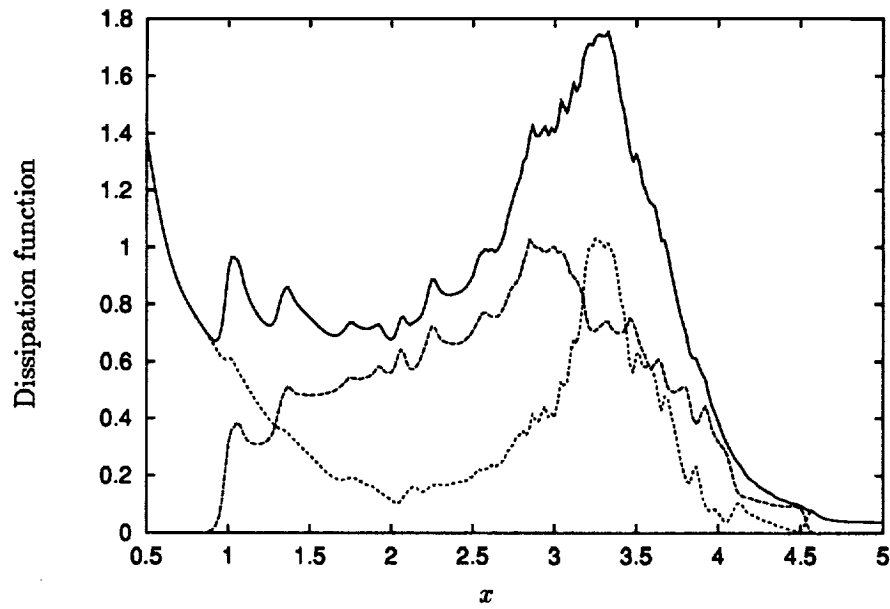
FIGURE 5. Dissipation function in the Reynolds stress budget, Eq. (14): total dissipation function (———), dilatational dissipation (— — — —), solenoidal dissipation (— - — - —).
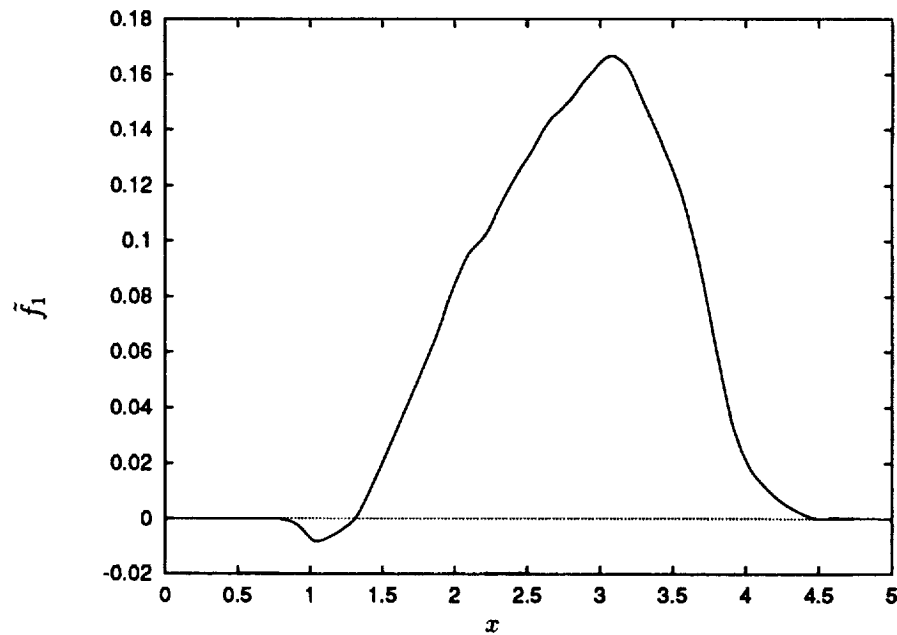

FIGURE 6. Reynolds flux $\tilde{f}_1 = \overline{\rho u_1'' c''}$ vs. distance x through the flame. Positive values indicate the presence of counter-gradient transport.

3. Scalar flux budget

The existence of counter-gradient transport in turbulent premixed flames has been confirmed both by experiment (Moss, 1980) and by theoretical analysis (Libby & Bray, 1981). Turbulent transport of heat and mass is found to occur in a direction opposite to that indicated by the sign of the mean gradient. In the present simulations this is equivalent to counter-gradient transport of the reaction progress variable c, whose mean gradient is positive in the x-direction and identically zero in the other two directions. Thus counter-gradient transport corresponds to positive values of the x-wise component of the turbulent Reynolds flux of reaction progress variable $\tilde{f}_1 = \overline{\rho u_1'' c''}/\bar{\rho}$.

A plot of this quantity is shown in Fig. 6, where it is evident that strong counter-gradient transport is indeed present throughout almost the entire flame brush, except for a small region at the leading edge in which gradient transport prevails. This result is consistent with previous findings (Libby, 1985).

It is possible to investigate the mechanisms behind the occurrence of counter-gradient transport by examining the budget of the Reynolds flux $\tilde{f}_1$. The balance equation for $\tilde{f}_1$ may be written as

$$\underset{(x)}{\frac{\partial \bar{\rho} \tilde{f}_1}{\partial t}} + \underset{(ix)}{\frac{\partial \bar{\rho} \tilde{u}_k \tilde{f}_1}{\partial x_k}} = \underset{(i)}{-\overline{\rho u_k'' u_1''} \frac{\partial \bar{c}}{\partial x_k}} \quad \underset{(ii)}{-\bar{\rho} \tilde{f}_k \frac{\partial \tilde{u}_1}{\partial x_k}} \quad \underset{(iii)}{+\overline{u_1'' w}} \quad \underset{(iv)}{-\frac{\partial \overline{\rho u_k'' u_1'' c''}}{\partial x_k}}$$

$$\underset{(v)}{-\overline{c''} \frac{\partial \bar{p}}{\partial x_1}} \quad \underset{(vi)}{-\overline{c'' \frac{\partial p'}{\partial x_1}}} \quad +\left(\underset{(vii)}{\overline{c'' \frac{\partial \tau_{1k}}{\partial x_k}}} \quad \underset{(viii)}{-\overline{u_1'' \frac{\partial J_k}{\partial x_k}}} \right) \quad (18)$$

Each term in this equation was evaluated individually from the DNS dataset and all are plotted in Fig. 7, with signs included as they appear in the equation. It should be noted that the simulated flame is not yet statistically stationary, but the budget is balanced within statistical error by the inclusion of the non-stationary term. It is clear from the figure that the dominant terms in the budget are those involving the pressure. The mean pressure term (v) is largest over more than half of the flame brush while the fluctuating pressure term (vi) is also significant, particularly over the forward portion of the flame brush. Both tend to promote counter-gradient transport by contributing towards positive values of the Reynolds flux. These results lend support to the theory that counter-gradient transport is produced by the local pressure gradient acting preferentially to accelerate the light, low-density burned gas more than the heavier unburned gas. In the present case the mean pressure gradient is negative, i.e. decreasing in the positive x-direction. Thus the burned gas is accelerated in the same direction and counter to the gradient of mean product mass fraction (and progress variable). It is worth noting that this mechanism would operate even in the absence of a contribution from the fluctuating pressure term.
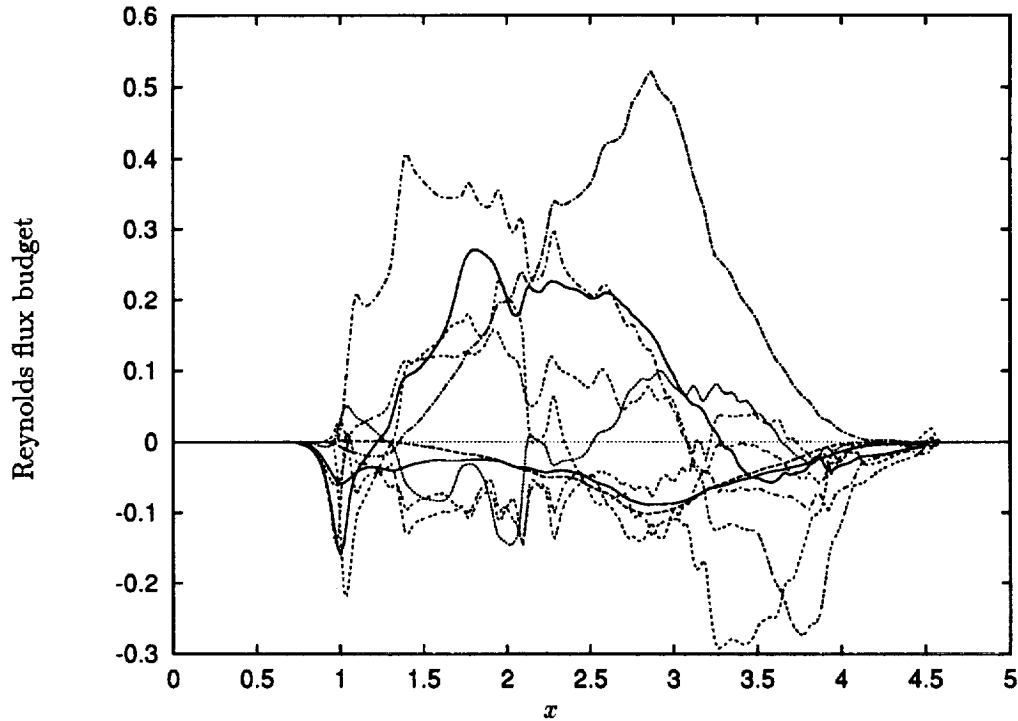
FIGURE 7. Reynolds flux budget, Eq. (18): production term (i) (——— , lower), production term (ii) (—————), velocity-reaction rate term (iii) (-----), third-moment term (iv) (········), mean pressure term (v) (————), fluctuating pressure term (vi) (- - - -), viscous term (vii) (- - - -), molecular diffusion term ($viii$) (--- --- -), convective term (ix) (--- ----- -), non-stationary term (x) (———— , upper).

The role of this term in further promoting counter-gradient transport is clear from the present results and indicates that this term is not negligible in this context.

None of the other source terms in the budget of Reynolds flux appears individually to exert a major influence on turbulent transport. The pressure terms are balanced by a combination of the other terms and there is no other dominant effect. Nevertheless it is interesting to examine the velocity-reaction rate term (iii) and the dissipation rate of the scalar flux (terms vii and $viii$). Both of these terms are driven by direct molecular effects in the presence of reacting gas and both are subject to the need for closure modeling. The velocity-reaction rate term is plotted in Fig.8. This term is non-zero only within the flame brush and appears noisy due to the relative lack of statistical sample associated with the presence of reaction. The correlation becomes negative towards the rear of the flame, reflecting the tendency of the velocity fluctuation magnitude to increase even as the reaction rate is falling.

The dissipation terms account for the removal of Reynolds flux due to viscous effects (term vii) and to molecular diffusion (term $viii$) and are plotted in Fig. 9. Both are non-zero only in the presence of reaction and are noisy for reasons given
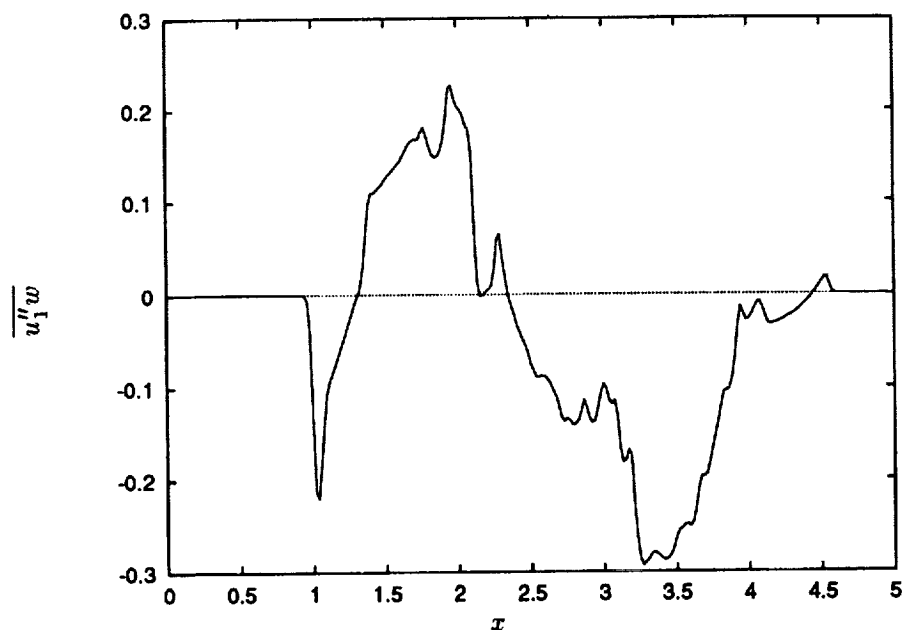
FIGURE 8.   The velocity-reaction rate correlation $\overline{u_1''w}$ (term iii) vs. distance x through the flame.
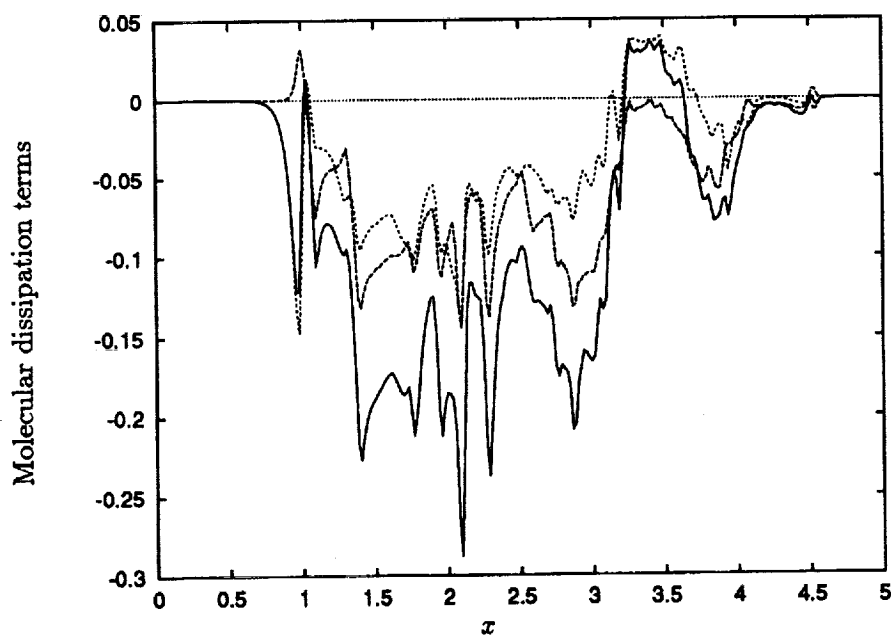

FIGURE 9.   Dissipation terms in the Reynolds flux balance Eq. (18), plotted vs. distance x through the flame. Viscous term (vii) (-----), molecular diffusion term ($viii$) (- - - - -), total dissipation ($vii + viii$) (———).

above. Each has a predominantly negative sign and acts as a mild sink throughout the flame brush. In the present case their magnitudes are very similar indicating that viscous and diffusional effects are of roughly equal importance in this flame.

4. BML Decompositions

The BML formalism is based on the premise that the laminar flamelets occurring within the turbulent flame brush are thin in the sense that the pdf of the progress variable is dominated by the entries at zero and unity, with little contribution from the interior part of the distribution. This has been checked using DNS by evaluating the weight functions α, β and γ corresponding respectively to unburned reactants, fully-burned products and material undergoing reaction. Results for these quantities are shown in Fig. 10. It is clear that γ is very much smaller than α and β throughout almost the entire flame brush, providing emphatic confirmation that the BML assumption is indeed valid in this flame.

The only exceptions occur near to the leading edge of the flame brush where it is clear that $\beta \to 0$ faster than γ, and at the trailing edge where $\alpha \to 0$ faster than γ. The maximum value of γ is about 0.15, attained near the center of the flame brush. Terms multiplying γ in several of the key BML expressions have been evaluated also and are generally found to be small.
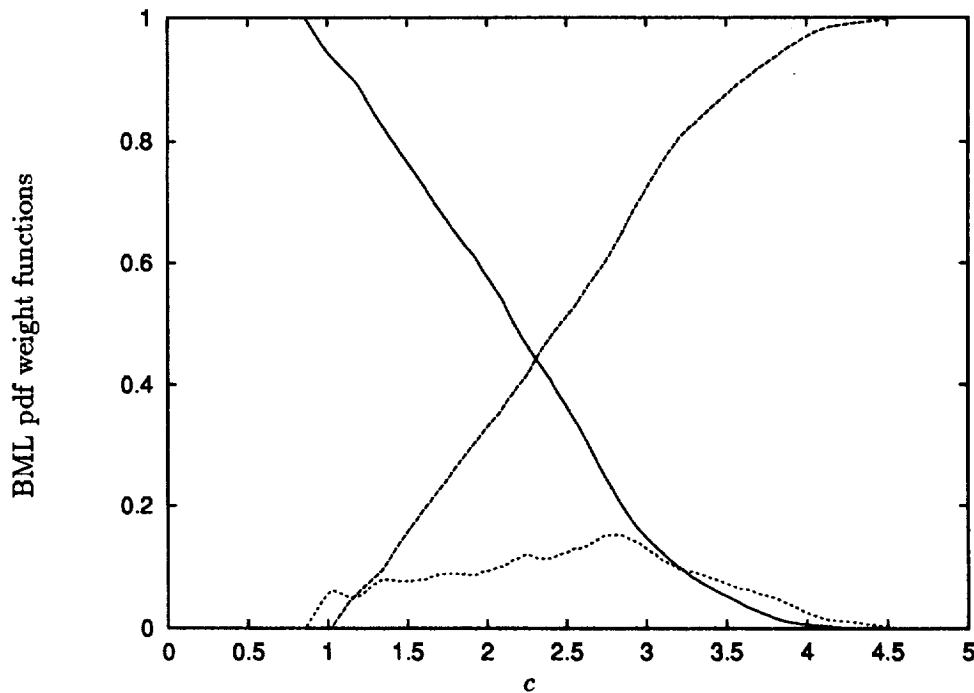

FIGURE 10. The weight functions α, β and γ in the BML pdf of progress variable c plotted against distance x through the flame. Reactant weight function α (————), product weight function β (— — — —), reacting material weight function γ (- - - - -).

The BML formalism may be used to decompose all of the second- and third-moment unconditional statistics of interest in terms of conditional statistics of lower order. For example, a covariance such as the Reynolds flux $\tilde{f}_1$ may be expressed in terms of a difference of conditional means:

$$\tilde{f}_1 = \overline{\rho u_1'' c''} \Big/ \bar{\rho} = \tilde{c}(1 - \tilde{c})(\bar{u}_{1P} - \bar{u}_{1R}) \tag{19}$$

where subscripts P and R indicate product and reactant, respectively. The conditional reactant and product mean velocities are shown in Fig. 11. The abrupt fall to zero at the ends is due to a lack of statistical sample: there is no more reactant (product) on which to condition as $c \rightarrow 1(0)$. It is interesting to note that there is no tendency of the conditional velocities or their difference to approach some asymptotic value at either limit. Checks were carried out to ensure that the results were insensitive to the choice of conditioning levels: this was confirmed for threshold values of c set at (0.01, 0.99), (0.05, 0.95) and (0.10, 0.90). Sample sizes were also checked and found to be adequate for the evaluation of the conditional means. Clearly the conditional difference $\bar{u}_{1P} - \bar{u}_{1R}$ is positive throughout most of the flame brush, implying through Eq.(19) that the Reynolds flux is positive and that counter-gradient diffusion is to be expected.

The BML formalism becomes particularly valuable in treating the unclosed third-moment correlations which appear in the balance equations for the Reynolds stresses and fluxes. Expressions for these terms are given in Bray *et al.* (1985) as

$$\begin{aligned}
\overline{\rho u_i'' u_j'' u_m''} \Big/ \bar{\rho} = \tilde{c}(1 - \tilde{c}) \big[&(1 - 2\tilde{c})(\bar{u}_{iP} - \bar{u}_{iR})(\bar{u}_{jP} - \bar{u}_{jR})(\bar{u}_{kP} - \bar{u}_{kR}) \\
&+ \left(\overline{u_i' u_j'}_P - \overline{u_i' u_j'}_R \right)(\bar{u}_{kP} - \bar{u}_{kR}) \\
&+ \left(\overline{u_j' u_k'}_P - \overline{u_j' u_k'}_R \right)(\bar{u}_{iP} - \bar{u}_{iR}) \\
&+ \left(\overline{u_i' u_k'}_P - \overline{u_i' u_k'}_R \right)(\bar{u}_{jP} - \bar{u}_{jR}) \big] \\
&+ (1 - \tilde{c}) \overline{u_i' u_j' u_k'}_R + \tilde{c} \overline{u_i' u_j' u_k'}_P + O(\gamma)
\end{aligned} \tag{20}$$

and

$$\begin{aligned}
\overline{\rho u_i'' u_j'' c''} \Big/ \bar{\rho} = \tilde{c}(1 - \tilde{c}) \big[&(1 - 2\tilde{c})(\bar{u}_{iP} - \bar{u}_{iR})(\bar{u}_{jP} - \bar{u}_{jR}) \\
&+ \left(\overline{u_i' u_j'}_P - \overline{u_i' u_j'}_R \right) \big] + O(\gamma)
\end{aligned} \tag{21}$$

In each case the third-moment quantity is decomposed as a series of terms involving mainly first- and second-moment conditional differences. This decomposition is central to the BML closure approach since only the conditional quantities need to be modeled, and these contain no contribution arising from density change. In order to check the decomposition, every quantity in each of these expressions was evaluated from the DNS database, and comparisons between the exact and the decomposed
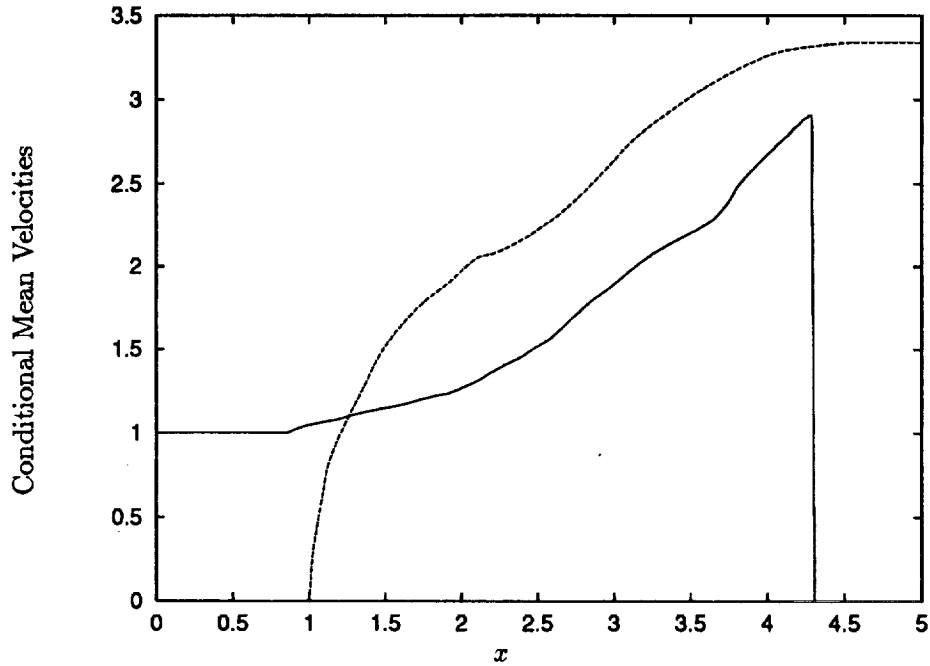
FIGURE 11. Conditional reactant and product mean velocities $\bar{u}_{1R}$ (———) and $\bar{u}_{1P}$ (————) plotted against x distance x through the flame.

results are shown in Fig. 12a for the Reynolds stress component $\overline{\rho u_1'' u_1'' u_1''}/\bar{\rho}$ and in Fig. 12b for the flux component $\overline{\rho u_1'' u_1'' c''}/\bar{\rho}$. Agreement is very good in each case over almost the entire flame brush, and the accuracy of the BML decomposition is verified. The third-moment stress remains non-zero outside the flame brush due to contributions from the conditional third moments. The third- moment flux by contrast is non-zero only within the flame brush, and there are discrepancies between exact and decomposed values at the leading and trailing edges. These are due once again to a lack of conditional sample as $c \to 0,1$. All ten independent components of the third-moment stress were evaluated and compared, as were all six independent components of the third-moment flux, and the same degree of agreement was apparent in all cases.

5. BML Modeling

BML closure modeling is based on balance equations for the second-moment Reynolds stresses and fluxes. These balance equations contain divergences of the third-moment terms as decomposed in Eqs. (20) and (21) above, and hence closure models are required for the unknown conditional differences. The conditional velocity differences $(\bar{u}_{1P} - \bar{u}_{1R})$ may be evaluated from the Reynolds fluxes $\tilde{f}_i$ using Eq. (19), and hence require no modeling.

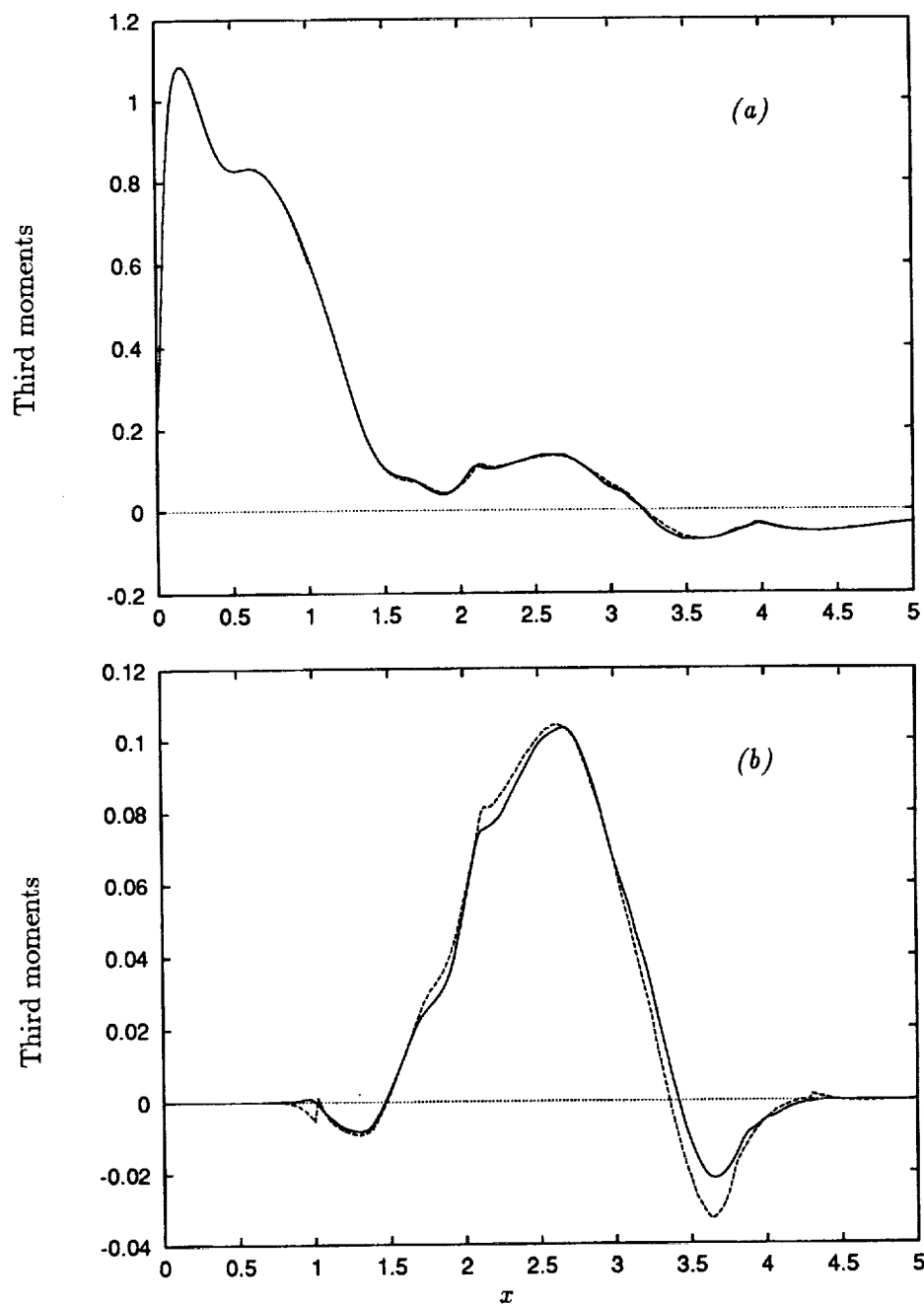The only terms remaining to be modeled are the differences of the conditional

$C \cdot 2$

FIGURE 12.   Decomposition of third-moment terms. Exact (———) and BML-decomposed (—————) forms plotted together for comparison. (a) Third-moment stress component $\overline{\rho u_1'' u_1'' u_1''}/\bar{\rho}$. (b) Third-moment flux component $\overline{\rho u_1'' u_1'' c''}/\bar{\rho}$
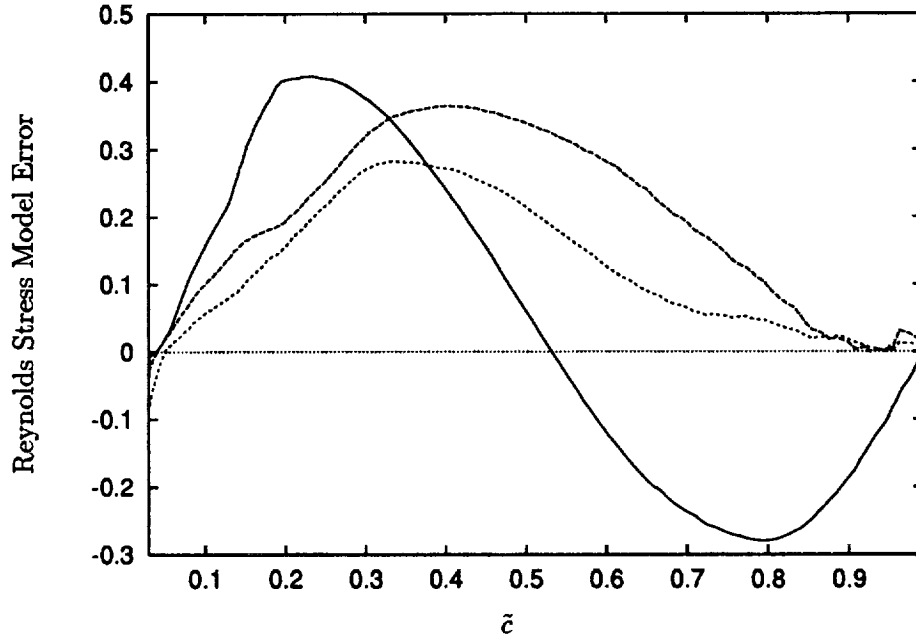
FIGURE 13. Errors in the modeled differences in conditional Reynolds stresses, Eq. (22): 11 (———), 22 (- - - - -), 33 (- - - - -). The errors are normalized by the difference between the maximum and minimum value over the whole range.

second-moment and third-moment stresses. A simple linear fit to model the difference in second moment stress has been proposed by Bray *et al.* (1985):

$$\left(\overline{u_i' u_j'}_P - \overline{u_i' u_j'}_R\right) \approx [(1 - \kappa_1)\,\tilde{c} + (\kappa_0 - 1)(1 - \tilde{c})]\,\frac{\overline{\rho u_i'' u_j''}}{\bar{\rho}} \tag{22}$$

where the constants κ_0 and κ_1 are allowed to vary with (i,j). This model was motivated by the requirement that the total Favre-averaged Reynolds stresses reduce to the conditional stresses at the edges of the flame brush: $\tilde{c} \rightarrow 0, 1$. This requirement also provides a means to evaluate the κ terms.

The κ terms were evaluated using the DNS data and the results are shown in Fig. 13. The figure shows the error of the modeled terms for the three normal stresses. By construction, the errors go to zero near the boundaries of the flame. The exact limits $\tilde{c} \rightarrow 0, 1$ could not be used to find the κ terms since the sample rates were too low. However, at least for the normal stresses, the κ values approached the limits fairly smoothly and were readily estimated. The errors plotted in Fig. 13 show that a linear fit is not very accurate. The terms would be better modeled by a second order fit for the tangential stresses and a third order fit for the normal stresses. However, further theoretical work is needed before such ad-hoc models are developed.

A generalized gradient-transport model has been proposed for modeling the differences of the conditional third-moment stresses (Bray *et al.* 1985):
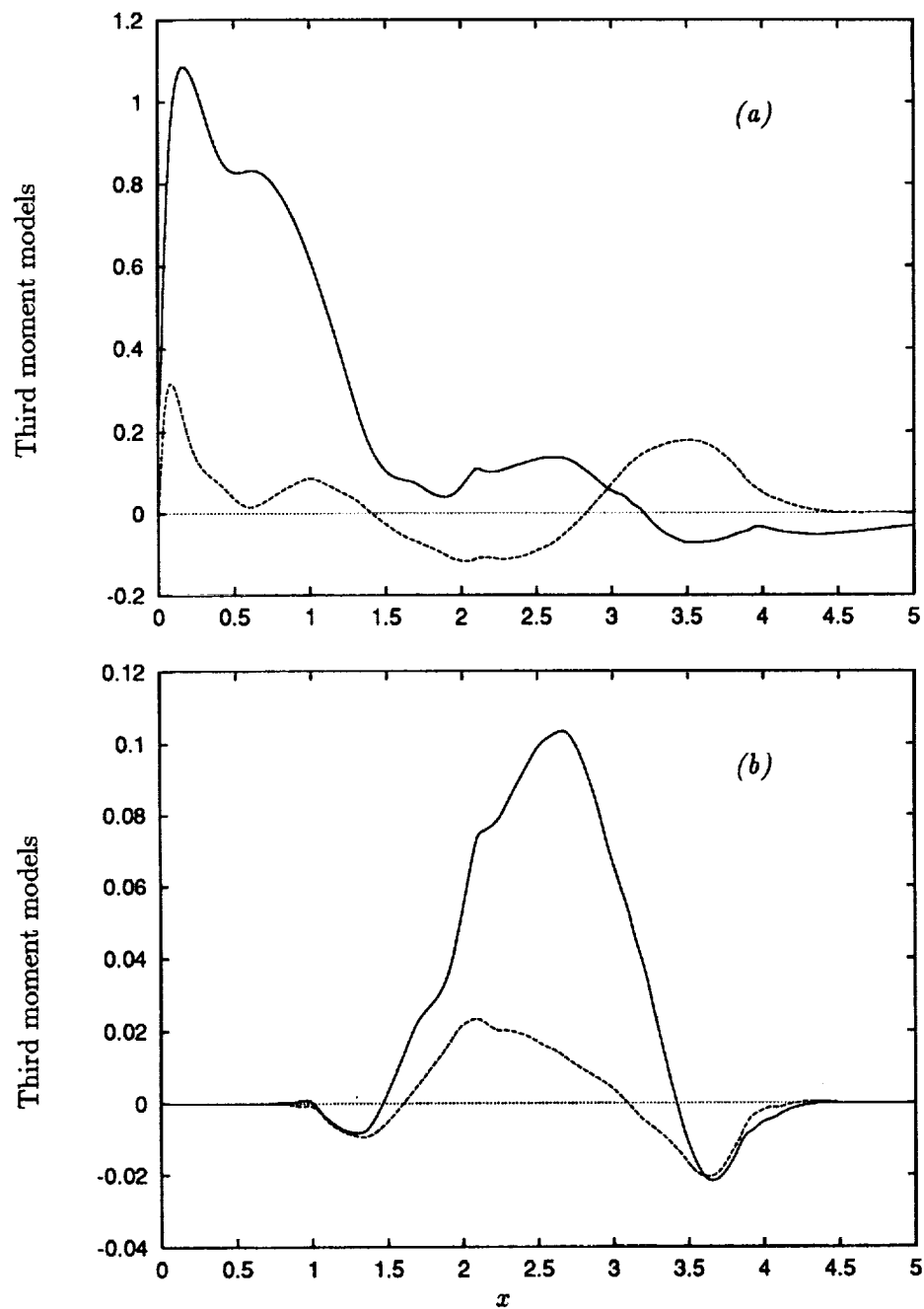
FIGURE 14.   Modeling of third-moment terms. Exact (————) and modeled
(— — — —) forms plotted together for comparison. *(a)* Third-moment stress compo-
nent $\overline{\rho u_1'' u_1'' u_1''}/\bar{\rho}$. *(b)* Third-moment flux component $\overline{\rho u_1'' u_1'' c''}/\bar{\rho}$.

$$(1 - \tilde{c})\,\overline{u_i'u_j'u_k'}_R + \tilde{c}\,\overline{u_i'u_j'u_k'}_P \approx -c_s\frac{\tilde{k}}{\tilde{\varepsilon}}\frac{\overline{\rho u_k''u_m''}}{\bar{\rho}}\frac{\partial}{\partial x_m}\left(\frac{\overline{\rho u_i''u_j''}}{\bar{\rho}}\right) \qquad (23)$$

All of the terms in Eqs. (20) and (21) which require modeling according to eqs.(22) and (23) have been evaluated from the DNS data and assembled to yield modeled third-moment stress and flux components $\overline{\rho u_1''u_1''u_1''}/\bar{\rho}$ and $\overline{\rho u_1''u_1''c''}/\bar{\rho}$, and the results are plotted in Fig. 14. The agreement of the modeled terms with their exact equivalents is poor and contrasts strongly with the excellent agreement obtained using the BML decomposition only. Both the conditional stress sub-model and the third-moment gradient diffusion sub-model are seen to be seriously deficient, failing to capture even the qualitative trends of the exact third-moment stress. Some evidence of the correct trend is present in the comparison for the third-moment flux, but quantitative agreement is not achieved. Again, all ten independent third-moment stresses and all six independent third- moment fluxes were evaluated, but the agreement remained comparably poor in all cases. Clearly the present sub-models are in need of considerable improvement.

6. Conclusions

The DNS data have been used to identify several important physical effects regarding turbulent transport occurring in premixed flames. Probably the most significant is counter gradient transport of the scalar flux. This was found previously in experiments (Moss, 1980) and predicted by theoretical analysis (Libby & Bray, 1981). The DNS results help confirm that pressure effects are the major contribution to counter gradient transport.

The DNS results also revealed the importance of pressure terms in Reynolds stress transport. The mean pressure gradient term dominates, but pressure transport and pressure dilatation are also very important. Dissipation, which is a major sink in the Reynolds stress budget, was found to be composed of both solenoidal and dilatational terms. The DNS data showed both terms to be significant.

Results have been obtained from the DNS which allow thorough validation of the BML model formalism in a statistically planar turbulent premixed flame. The principal assumption of BML - that the pdf of the progress variable is strongly bimodal - has been checked and found to be valid throughout the simulated flame. All of the second-moment and third-moment Reynolds stress and Reynolds flux components have been evaluated and compared with their equivalents obtained using the BML formalism. Very good agreement is observed where terms obtained through the BML decomposition are themselves evaluated from the DNS. This confirms that BML provides a valid theoretical framework for the treatment of premixed turbulent flames.

By contrast, agreement is poor where the decomposed terms are evaluated using currently available model expressions. Thus, while the framework has been found to be satisfactory, the modeling itself must be improved. Much of the information which will be required to underpin the necessary model development is contained within the present DNS dataset. Its exploitation will form the next major task.

REFERENCES

ANTONIA, R. A., DJENIDI, L., & SPALART, P. R. 1994 Anisotropy of the dissipation tensor in a turbulent boundary layer. *Physics of Fluids.* **6-7**, 2475-2479.

BRAY, K. N. C. & CANT, R. S. 1991 Some Applications of Kolmogorov's Turbulence Research in the Field of Combustion. *Proc. R. Soc. Lond. A.* **434**, 217-240.

BRAY, K. N. C., LIBBY, P. A. & MOSS. J. B. 1985 Unified Modeling Approach for Premixed Turbulent Combustion - Part I: General Formulation. *Combust. Flame.* **61**, 87-102.

JONES, W. P. 1980 Models for Turbulent Flows with Variable Density and Combustion *Prediction Methods for Turbulent Flows*, W. Kollmann, Ed., Hemisphere Publishing Corp.

LEE, S., LELE, S. K. & MOIN, P. 1991 Simulations of Spatially Decaying Compressible Turbulence. Center for Turbulence Research, NASA Ames/Stanford Univ., Manuscript 126.

LELE, S. K. 1992 Compact Finite Difference Schemes with Spectral-like Resolution. *J. of Comp. Physics.* **103**, 16-42.

LIBBY, P. A. & BRAY, K. N. C. 1981 Countergradeint Diffusion in Premixed Turbulent Flames. *AIAA Journal.* **19-2**, 205-213.

LIBBY, P. A. 1985 Theory of Normal Premixed Turbulent Flames Revisited. *Prog. Energy. Combust. Sci..* **11**, 83-96.

McMURTRY, P. A., JOU, W.-H., RILEY, J. J.& METCALFE, R. W. 1986 Direct Numerical Simulations of a Reacting Mixing Layer with Chemical Heat Release. *AIAA Journal.* **24-6**, 962-970.

MOSS, J. B. 1980 Simultaneous measurements of concentrations and velocity in an open premixed turbulent flame. *Combust. Sci. Tech.* **22**, 119-129.

RUTLAND, C. J., FERZIGER, J. H.& CANTWELL, B. J. 1989 Effects of Strain, Vorticity, and Turbulence on Premixed Flames. *Report No. TF-44.* Thermosciences Division, Dept. of Mechanical Engineering, Stanford University.

SCHUMANN, U. & PATTERSON, G. S. 1978 Numerical study of pressure and velocity fluctuations in nearly isotropic turbulence. *J. Fluid Mech.* **88-4**, 685-709.

STRAHLE, W. C. 1983 Velocity-Pressure Gradient Correlation in Reactive Turbulent Flows. *Combust. Sci. Tech.* **32**, 289-305.

TROUVÉ, A. & POINSOT, T. 1993 The Evolution Equation for the Flame Surface Density in Turbulent Premixed Combustion, Center for Turbulence Research, NASA Ames/Stanford Univ., Manuscript 140.

ZHANG, S. & RUTLAND, C. J. 1994 Pressure Effects in Turbulent Trasnport of Premixed Flames. *Submitted to Comb. and Flame.*

ZHANG, S. 1994 Simulations of Premixed Flames with Heat Release, Ph.D. Thesis, Dept. of Mech. Engr., Univ. of Wisconsin.